RSC Advances

Ru(II)-polypyridyl complexes grafted silica nanohybrids: Versatile hybrid materials for Raman spectroscopy and photocatalytic activity

Journal:	*RSC Advances*
Manuscript ID:	RA-ART-11-2014-014202.R1
Article Type:	Paper
Date Submitted by the Author:	08-Jan-2015

Complete List of Authors:	Narayanasamy, Vilvamani; Delhi University, Chemistry Department Gupta, Rinkoo; South Asian University, Faculty of Life Sciences and Biotechnology Awasthi, Satish; Delhi University, Delhi, Chemistry Department; Delhi University, Chemistry Department

Cite this: DOI: 10.1039/c0xx00000x

www.rsc.org/xxxxxx

ARTICLE TYPE

Ru(II)-polypyridyl complexes grafted silica nanohybrids: Versatile hybrid materials for Raman spectroscopy and photocatalytic activity†

Narayanasamy Vilvamani,[a] Rinkoo Devi Gupta[*b] and Satish Kumar Awasthi[*a]

Received (in XXX, XXX) Xth XXXXXXXXX 20XX, Accepted Xth XXXXXXXXX 20XX

DOI: 10.1039/b000000x

Ruthenium(II)-polypyridyl complexes grafted silica nanohybrids with and without silver nanoparticle (Ag NP) as core-shell nanohybrids were prepared by reacting with different coupling reagents 3-aminopropyl-trimethoxysilane (3-APTMS) and 3-iodopropyltrimethoxysilane (3-IPTMS). The morphological features of the resulting surface grafted silica nanohybrids were studied using various electron microscopic techniques (TEM, STEM, SEM, EDS) and their chemical components were analysed using spectral techniques such as mass spectrometry, UV-vis, Fourier transform-infrared (FT-IR) spectroscopies and thermogravimetric analysis (TGA). Photoluminescence (PL) studies of functionalized silica nanohybrids in solution and solid state proved them as luminescent nanohybrids. The molecular vibrational bands of covalently grafted Ru(II)-polypyridyl complexes on silica nanohybrids and Ag@SiO_2 core-shell nanohybrid were studied using Raman spectroscopy. Thus obtained Ru(II)-polypyridyl complex functionalized silica nanohybrids were utilized as a photocatalyst for Rhodamine 6G degradation under visible light illumination. The presence of thick SiO_2 nanoshell over Ag NP surface limits direct charge transfer to covalently grafted Ru(II)-polypyridyl complex and Ag NP proved as a plasmonic photosensitizer for enhanced Rhodamine 6G degradation and molecular probing substrate for Raman spectroscopy. Among functionalized silica nanohybrids, Ag@SiO_2 core-shell nanohybrid showed enhanced photocatalytic activity towards Rhodamine 6G degradation than other functionalized silica nanohybrids without Ag NP core and bare MCM-41 SiO_2 NP.

1. Introduction

Functionalized silica nanohybrids with noble metal nanoparticles initiated an enormous interest in the field of nanoplasmonics, cellular imaging and catalysis.[1-3] The combination of metal NP with SiO_2 NP as core-shell nanostructure has been used in many aspects in the field of nanotechnology because of tuneable visible range surface plasmon resonance of metal NPs and optical transparency, inertness, solubility and ensured metal core protection of SiO_2 in various polar and non-polar solvents.[4-5] The placement of SiO_2 nanoshell with silanol (-Si-OH) groups over metal NP surface furthermore extends an opportunity to functionalize its surface through the covalent bonding of molecules.[6] Additionally, silica nanohybrid with Ag NP core represents multicomponent material interface which often enhances the functional properties, and thus become more advantageous than its individual counterparts.[7] These combined properties make SiO_2 NP as ideal substrate for designing and making different functionalized nanohybrid materials with targeted novel applications.

The presence of Ag NP with size and shape dependent localized surface plasmon resonance (LSPR) in the visible region with suitable SiO_2 matrix in various chemical compositions made them as desirable photocatalysts for degrading organic pollutants and for various organic functional group conversions.[8-9] For example, Wu *et al.* followed one-pot template liquid phase methodology to develop N-doped titanium dioxide (TiO_2) nanorod arrays loaded with Ag NPs, which showed methyl blue (MB) degradation activity.[10] Yan *et al.* prepared Ag NPs loaded multiwalled carbon nanotubes (CNTs) and utilized them as photocatalyst to degrade Rhodamine B under visible light.[11] Further, Liang *et al.* prepared TiO_2 nanotubes using anodic aluminium oxide (AAO) as a template by applying atomic layer deposition methodology and then Ag NPs deposited over nanotubes as an electron trapper to make the slower electron-hole recombination during the photocatalytic process.[12] Xie *et al.* demonstrated photoelectrochemical properties of Ag NPs loaded TiO_2 nanotubes using pulse current deposition methodology and showed enhanced photoelectrocatalytic activity towards degradation of methyl orange under UV light irradiation.[13] Recently, Wang *et al.* prepared tubular heterostructure composed of TiO_2-SiO_2 and showed photocatalytic activity on Rhodamine 6G under UV light irradiation.[14] These reports clearly revealed the importance and role of Ag NPs based heterostructure nanomaterials in photocatalytic processes. However, the important point is that, the direct contact of TiO_2 with Ag NP surface leads to the formation of passive silver oxide (AgO) layer, which declines photocatalytic performance of the resulting

nanomaterials. To overcome the above mentioned issues, SiO_2 nanoshell placed over Ag NP surface followed by grafting suitable photoactive molecules on SiO_2 surface represents promising functionalized plasmonic photocatalysts.[15] Presently, grafting the surface of silver@silica core-shell NPs ($Ag@SiO_2$ NPs) using photoactive molecules has drawn most attention because of remarkable optoelectronic performance in organic solar cells.[16] Recently, Mishra *et al.* studied in detail about the placement of eosin dye on various nanoscaled SiO_2 coated Ag NPs island films and showed that distance dependent Ag NP plasmon enhanced luminescence of the resulting functionalized hetero-nanostructures and the influence of SiO_2 coating thickness on luminescence properties.[17] We have been working on design and development of functionalized monolayers on various surfaces such as p+ silicon wafer, glass and nanoparticles (Au, Ag) for various practical applications.[18-21] Because of an increased attention towards the fascinating properties of silica based multifunctional nanohybrids,[22] we got motivated and prepared different Ru(II)-polypyridyl complexes with different functional groups and then grafted them on SiO_2 NPs, $Ag@SiO_2$ core-shell NPs and studied their optical, photocatalytic properties. Further, we demonstrated optically that localized surface plasmon resonance (LSPR) of Ag NP core inside SiO_2 nanoshell act as a plasmonic photosensitizer to enhance the absorption cross-section of Ru(II)-polypyridyl complex grafted on SiO_2 NP surface. The photocatalytic activity of different silica nanomaterials with and without surface bound Ru(II)-polypyridyl complexes showed the progressive enhancement with control experiment. This work illustrates the precise architecture of nanohybrids with tailor-made silica surface functionalized with photoactive molecular sites for time dependent surface plasmon enhanced Raman scattering (PERS) studies and plasmonic photocatalytic processes.

2. Experimental section

2.1 Materials

Tetraethylorthosilicate (TEOS, 98%), 3-iodopropyltrimethoxy-silane (3-IPTMS, >95%), 3,4,7,8-tetramethyl-1,10-phenanthroline (>99%), 4-formylbenzoic acid (97%), 4-hydroxybenzaldehyde (98%), N-hydroxysuccinimide (NHS, 98%), dicyclocarbodiimide (DCC, 99%) were received from Sigma-Aldrich. Silver nitrate (99+%), 3-aminopropyltrimethoxysilane (3-APTMS, 98%) were received from Alfa Aesar, Rhodamine 6G from Loba Chemie, dry acetonitrile, absolute ethanol received from J. H. Inter. trade co. Ltd, China. Toluene was distilled over sodium/benzophenone mixture, while dichroloromethane was distilled over calcium chloride and dried over 3Å molecular sieves.[23] Dimethylsulfoxide (DMSO, AR) was received from SISCO research laboratories, India. Ammonia (~30%) from Fischer scientific, 1,10-phenanthroline (1,10-phen, 99%) from Spectrochem, SiO_2 NPs (10 nm size, 30% suspension) were received from Reinste, India. All chemicals were used as received without any further purification. 1,10-Phen-5,6-dione,[24] 4-(1H-imidazo-[4,5-f][1,10]phenanthrolin-2-yl) benzoic acid (IPBA),[25] 4-(1H-imidazo[4,5-f][1,10]phenanthrolin-2-yl)phenol (IPP),[26] *cis*-bis(2,2'-bipyridine)ruthenium(II)dichloride, *cis*-bis(1,10-phen)ruthenium(II)dichloride and *cis*-bis(3,4,7,8-tetramethyl-1,10-phen)ruthenium(II) dichloride,[27] $Ru(2,2'\text{-bpy})_2(IPBA).2PF_6$, $Ru(1,10\text{-phen})_2(IPBA).2PF_6$[28] were prepared as described in the literature. All aqueous solutions were prepared using double distilled water.

2.2 Characterizations

High resolution transmission electron microscopic (HRTEM) images and Fast Fourier transform (FFT) patterns were obtained using a transmission electron microscope (TECNAI G^2 T30) working at 300 kV accelerating voltage coupled with energy dispersive spectroscopy (EDS) facility. Scanning transmission electron microscopic high angle annular dark field (STEM-HAADF) images were captured in bright field mode. Scanning electron microscopic (SEM) images were taken using EVO/MA 15 ZEISS instrument operating at 20.0 kV accelerating voltage and FEI Quanta 200-3D dual beam ESEM with resolution of 3 nm at 30 kV accelerating voltage. ^{1}H NMR spectra of ligands and complexes were recorded using a Jeol ECX 400 MHz spectrometer working at field strength of 400 MHz. Mass spectra were recorded using Autoflex III Smartbeam MALDI-time-of-flight instrument from Bruker Daltonics (Bremen, Germany), equipped with a solid-state laser (λ= 355 nm) and spectra were collected from 200 laser shots in positive ion mode using matrix (2,5-dihydroxybenzoic acid (ACN/TFA (0.1%) 2:1 v/v) and the electrospray ionization mass spectra (ESI-MS) collected using Micromass instrument (Model-KC455, UK limited) with appropriate carrier solvent. The IR spectral data were recorded using KBr pellets on a Shimadzu IR435 spectrometer (400-4000 cm^{-1}) and on PerkinElmer FT-IR spectrometer (ZnSe crystal, 600-4000 cm^{-1}). Thermogravimetric analyses (TGA) were recorded using a PerkinElmer Diamond TG/DTA thermogravimetric/ Differential thermal analyzer with α-alumina powder as a reference under N_2 gas atmosphere. Elemental analysis was measured on an Elementar Analysensysteme GmbH varioEL V3.00. The electronic absorption spectra of all samples were recorded using Jasco V-670 spectrophotometer at room temperature. The emission spectra were collected from a Varian Cary Eclipse fluorescence spectrophotometer working at room temperature. Raman scattering and solid state photoluminescence (PL) studies were carried out using a Horiba Jobin Yvon Lab Ram HR 800 system operating at laser excitation of 488 nm. Renishaw invia Raman spectrometer operating at laser excitation 785 nm (HPNIR diode) was used to record Raman scattering of silica nanohybrids.

2.3 Synthesis of Ru(II)(3,4,7,8-tetramethyl-1,10-phen)$_2$(IPP).2PF$_6$

Cis-Ru(3,4,7,8-tetramethyl-1,10-phen)$_2$Cl$_2$.2H$_2$O (0.1 mmol, 68.0 mg) was refluxed with IPP ligand (0.1 mmol, 31.2 mg) in 10 ml ethanol/water (3:1 v/v) mixture for 6hr under N_2 atmosphere with constant stirring. During the course of the reaction, the solution colour changed from purple to dark red in colour. After completion of the reaction, the resulting solution cooled to room temperature and filtered to remove unreacted portions over whatman filter paper. Then, $2Cl^-$ ion exchanged with $2PF_6^-$ by adding 2 ml saturated solution of NH_4PF_6. The title compound was obtained as reddish orange precipitate, filtered out and washed thrice with diethyl ether. Yield (64 %, 58 mg). ^{1}H NMR (400 MHz, CD_3CN): δ 8.87 (dd, J = 8.1 Hz, 2H), 8.35 (d, J = 7.7

Hz, 4H), 8.1(d, J = 8.1 Hz, 2H), 7.84 (m, 2H), 7.69 (m, 4H), 7.57 (m, 2H), 6.99 (d, J = 7.9 Hz, 2H), 2.77 (s, 6H), 2.74 (s, 6H), 2.22 (s, 6H), 2.18 (s, 6H). FTIR (ZnSe, cm^{-1}): 3636 (m), 3512 (b), 3377(b), 2924 (w), 1695 (s), 1614 (s), 1481 (s), 1451(s), 1425 (s), 1388 (m), 1364 (m), 1276 (w), 1195 (m), 1175 (w), 1010 (b), 979 (s), 832 (s), 742 (s), 721(s), 555 (s). UV λ_{max} (CH_3CN, ε mol^{-1} cm^{-1})/ nm): 208 (73251), 269 (87528), 426 (15872), 467 (13574). MALDI-TOF MS (m/z) = 885.155. EA: (calc.) C, 66.94; N, 12.25; H, 4.85 (found) C, 66.58; N, 13.19; H, 4.96%.

2.4 Synthesis of MCM-41 SiO_2 NPs[29]

1.4 ml of NaOH (2N) solution was added with 192 ml water to bring pH = 12.16, and then CTAB (0.4 g) was dissolved homogeneously. To this basic surfactant solution, 2 ml TEOS was added drop wise at once with vigorous stirring on oil bath at 80˚C, then reflux continued for 2hr. After cooling to room temperature, the resulting wet silica centrifuged at 10,000 rpm 10 min and washed thrice with water. Moisture free MCM-41 SiO_2 NP was obtained by drying at 110˚C for 48hr and then calcinated at 873 K for 5hr. The resulting MCM-41 SiO_2 NPs morphological features were characterized using electron microscopies.

2.5 Ru(II)-polypyridyl complexes grafting on SiO_2 NPs[30]

The reaction mixture containing 1.0 mmol of Ru(2,2'-bpy)$_2$(IPBA).2PF_6 complex with NHS (0.6 mmol) and DCC (0.8 mmol) were dissolved in 10 ml dried acetonitrile, then stirred at room temperature for 12hr under N_2 gas atmosphere. The resulting red solution containing white precipitate was filtered out and the filtrate was concentrated under vacuum to 5 ml and dry toluene (5 ml) was added with 3-APTMS (1.1 mmol) and refluxed it for 24hr at 90˚C. The resulting reaction mixture was cooled to room temperature, washed with n-pentane to remove unreacted 3-APTMS, dried under vacuum to get orange powder of silylated Ru(II)(2,2'-bpy)$_2$(IPBA).2PF_6. 30% SiO_2 NPs suspension (200 µl) was added to 3-APTMS coupled Ru(II)(2,2'-bpy)$_2$(IPBA).2PF_6 in ethanol: water (1:1) under sonication for 5 minutes and refluxed for 24hr. The resulting functionalized silica nanohybrids separated by centrifugation at 12,000 rpm for 10 minutes and washed thrice (10 ml per washing) with the same solvent. Thus obtained functionalized silica nanohybrids dried and stored under vacuum at room temperature. Thus obtained Ru(II)(2,2'-bpy)$_2$(IPBA).2PF_6 complex grafted silica nanohybrid labelled as Si-RuH1 nanohybrid I. For Ru(II)(1,10-phen)$_2$(IPBA).2PF_6 complex grafting over SiO_2 NP, the same procedure followed and the resulting functionalized silica nanohybrid coded as Si-RuH2 nanohybrid II.

2.6 Synthesis of Ag@SiO_2 core-shell NPs[31]

Citrate capped Ag NP was synthesized as reported in literature and used for making larger sized Ag NP core in Ag@SiO_2 core-shell NPs.[32] To 40 ml absolute ethanol, 8 ml of citrated capped Ag NP was added under stirring condition. After 5 minutes, 600 µl of ammonia solution (~30%) was added at once. To the resulting mixture, 200 µl of TEOS was added with vigorous stirring. After few minutes, the colloidal colour was changed from pale yellow to turbid white confirmed the formation of SiO_2 nanoshell on Ag NP surface under basic condition. The resulting colloidal solution was stirred constantly for 24hr at room temperature. The final Ag@SiO_2 core-shell NPs were separated from the reaction mixture by centrifugation (10,000 rpm for 10 min.) and repeatedly washed thrice with deionized water to ensure free from reactants. Thus obtained Ag@SiO_2 core-shell NP was dried in vacuum at 45˚C before using for further surface functionalization process.

2.7 Surface functionalization of Ag@SiO_2 core-shell NPs

2.0 mmol Ru(II)(3,4,7,8-tetramethyl-1,10-phen)$_2$(IPP).2PF_6 complex was silylated with 3-IPTMS (200 µl) in presence of dry acetonitrile (10 ml) under N_2 gas atmosphere for 16hr at 80˚C. The resulting 3-IPTMS coupled Ru(II)(3,4,7,8-tetramethyl-1,10-phen)$_2$(IPP).2PF_6 complex was cooled to room temperature. Then, Ag@SiO_2 core-shell NP (120 mg) was added along with 10 ml dry toluene and sonicated for 10 minutes, followed by refluxing at 90˚C for 24hr under N_2 atmosphere. Finally, Ru(II)(3,4,7,8-tetramethyl-1,10-phen)$_2$(IPP).2PF_6 complex grafted Ag@SiO_2 nanohybrid was isolated as an orange powder by centrifugation (10,000 rpm) for 10 minutes. Further, unreacted reactants from Ru(II)(3,4,7,8-tetramethyl-1,10-phen)$_2$(IPP).2PF_6 complex functionalized Ag@SiO_2 nanohybrid particles were removed by thoroughly washing thrice with anhydrous toluene, dichloromethane and ethanol. The resulting functionalized silica nanohybrid was dried and stored in vacuum at room temperature until further use. This functionalized nanohybrid was found to be leach-free and stable in wide range of solvents and coded as Ag@SiO_2 core-shell nanohybrid III.

2.8 UV-vis absorption and emission measurements

All Ru(II)-polypyridyl complex functionalized silica nanohybrids I, II, III were dissolved in 2.5 ml DMSO (1 mg per ml) and then 250µl homogenized colloids again dispersed in 2ml DMSO (~250 µg in 2ml). These homogeneous colloidal solutions were utilized for absorption and emission measurements at room temperature. The emission spectra were recorded by exciting silica nanohybrids I, II, III samples at $\lambda_{exc.}$ = 455, 450, 440 nm respectively.

2.9 Photocatalytic activity parameters[14, 32]

The evaluation of visible light photocatalytic activity of functionalized silica nanohybrids was performed by exposing Rhodamine 6G aqueous solutions under 500 W high-pressure halogen lamp visible light. The temperature of the reaction medium was fixed below 280 K by flowing cold methanol during the reaction period. In each reaction condition, the amount of photocatalyst added was 15 mg along with 30 ml of Rhodamine 6G solution with a concentration of 12.0 mg L^{-1} in a reaction setup. Prior to visible light illumination, photocatalyst-Rhodamine 6G mixture was magnetically stirred under dark condition for 1hr to attain adsorption-desorption equilibrium with Rhodamine 6G on the photocatalyst surface. After fixed time period, 2 ml of the reaction mixture was taken out and centrifuged (10,000 rpm, 10 min) to isolate the photocatalyst and the resulting supernatant with remnant Rhodamine 6G used for UV-vis absorption measurements. In order to check the degradation ability of the photocatalyst used, blank experiment was also carried out without catalyst. The degradation percentage (%) is reported as C/C_0, where C is the λ_{max} of Rhodamine 6G for every time period at a wavelength of 526 nm and C_0 is the initial concentration absorption. The degradation rate (η) is calculated

from the given formula (η) = $[(A_0\text{-}A)/A_0]*100$, where A_0 is the initial absorbance of Rhodamine 6G after the adsorption-desorption equilibrium without visible light exposure and A is the absorbance of Rhodamine 6G after each visible light exposure time.

3. Results and discussion

Citrate capped Ag NP (~15 nm) was synthesized by the Lee-Meisel method and utilized as a precursor to obtain larger Ag NP core inside of SiO_2 nanoshell.[33] UV-vis spectra of citrate capped Ag NP showed SPR band at 438 nm with spherical morphology confirmed by TEM imaging (Fig. S1).

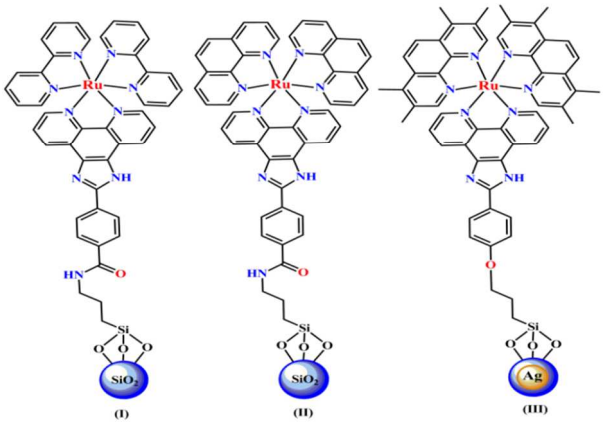

Fig. 1. Schematic view of various Ru(II)-polypyridyl complexes grafted silica nanohybrids (I, II, III).

Morphological changes of SiO_2 NPs and Ag@SiO_2 core-shell NPs were studied before and after functionalization with Ru(II)-polypyridyl complexes using electron microscopies (TEM, STEM, SEM). Blank Ag@SiO_2 core-shell NPs had 160-175 nm Ag NP core and 25-45 nm thick SiO_2 shell before grafting process. EDS profile & FFT pattern of bare Ag@SiO_2 core-shell NPs showed the presence of Ag, Si, O, Cu, C elements with crystalline surface (Fig. S2). The presence of bright Ag NP core differentiated from the thick SiO_2 shell by scanning transmission electron microscopy (STEM) and TEM images.

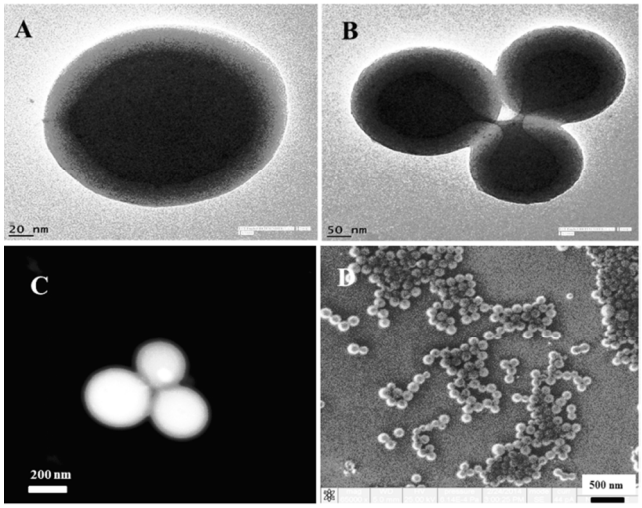

Fig. 2. Representative TEM (A, B), STEM (C), SEM (D) images showing bare Ag@SiO_2 core-shell NP morphological feature before grafting with Ru(II)-polypyridyl complex.

The uniform spherical shape of Ag@SiO_2 core-shell NP was confirmed from scanning electron microscopy (SEM), which is in well agreement with the result observed in TEM imaging (Fig. 2). After grafting 3-IPTMS coupled Ru(II)(3,4,7,8-tetramethyl-1,10-phen)$_2$(IPP). $2PF_6$, SiO_2 nanoshell thickness increased from ~45 nm to 60 ± 10 nm without affecting spherical morphology. Here, EDS profile confirmed the presence of Ru element along with Ag, Si, O, Cu, C elements (Fig. 3).

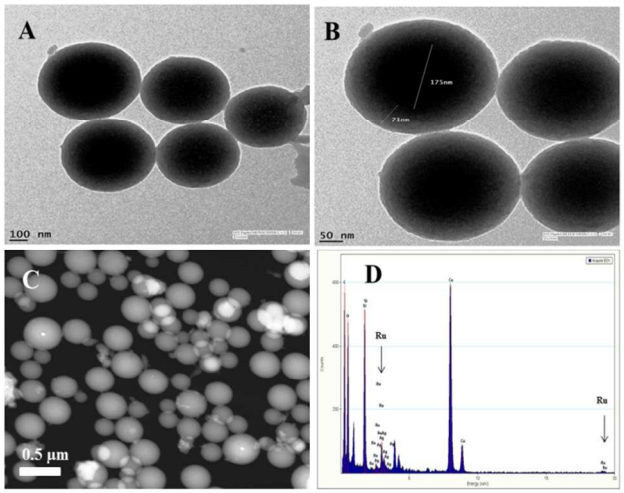

Fig. 3. A, B) Representative TEM images showing Ag@SiO_2 core-shell nanohybrid III with 3-IPTMS linked Ru(II)(3,4,7,8-tetramethyl-1,10-phen)$_2$(IPP).$2PF_6$; C) STEM image of Ag@SiO_2 core-shell nanohybrid III; D) EDS pattern of Ag@SiO_2 core-shell nanohybrid III showing Ru element along with Ag, Si, O, Cu, C elements.

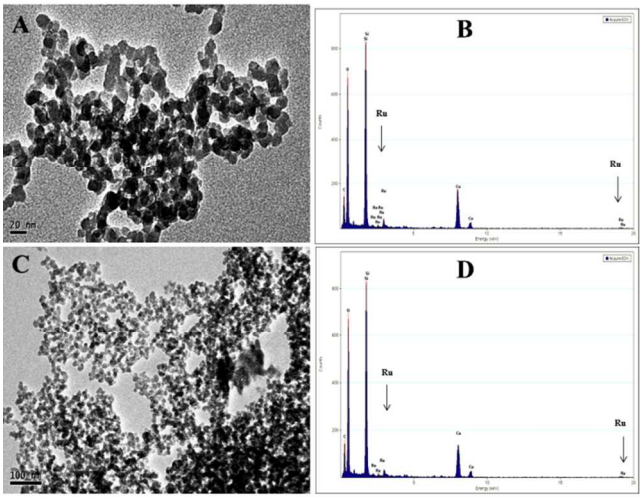

Fig. 4. A, B) Representative TEM image of Si-RuH1 nanohybrid I with 3-APTMS coupled Ru(II)(2,2'-bpy)$_2$(IPBA).$2PF_6$ with EDS profile; C, D) TEM image of Si-RuH2 nanohybrid II and EDS analysis showing presence of Ru, Si, O, Cu elements.

By comparing IR band positions of free Ru(II)(3,4,7,8-tetramethyl-1,10-phen)$_2$(IPP).$2PF_6$ with Ag@SiO_2 surface bound complex, the appearance of peak from 1320-1485 cm^{-1} confirmed the presence of covalently grafted Ru(II)(3,4,7,8-tetramethyl-1,10-phen)$_2$(IPP).$2PF_6$ but there are no such peaks in the finger print region of blank Ag@SiO_2 (Fig. S3). The scissor bending vibration peak of H-O-H noted at ~1630 cm^{-1} is due to the

presence of surface absorbed water in blank $Ag@SiO_2$ and $Ag@SiO_2$ core-shell nanohybrid III. The morphology studies of Si-RuH1 nanohybrid I and II confirmed the presence of surface grafted Ru(II)-polypyridyl complexes (Fig. 4).

The formation of 3-APTMS coupled Ru(II)(2,2'-bpy)$_2$(IPBA).2PF$_6$ complex was confirmed by FT-IR spectroscopy (Fig. S4A). The absorption peak at 2855 cm^{-1} corresponds to -CH_2- group of 3-APTMS. However, the appearance of two new peaks observed at 1606 and 1706 cm^{-1} hint towards the presence of -CONH- functional group formed as a result of coupling process. Similarly, Ru(II)(1,10-phen)$_2$(IPBA).2PF$_6$ complex silylated with 3-APTMS (Fig. S4B) showed the peaks at 1104, 1014 cm^{-1} which were assigned to asymmetric stretching of Si-O-Si, and peak at 1384 cm^{-1} for CH of MeO-Si- group substantiates the formation of coupling agent linked Ru(II)-polypyridyl complexes.[34-36]

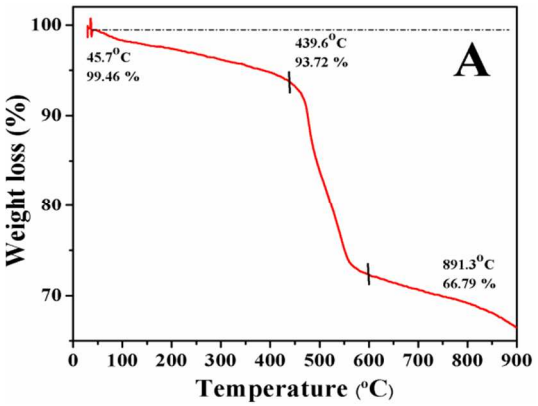

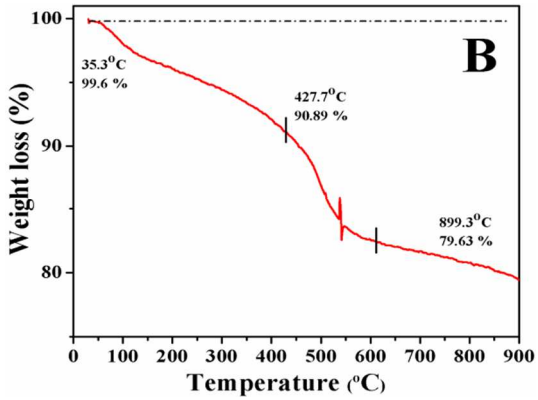

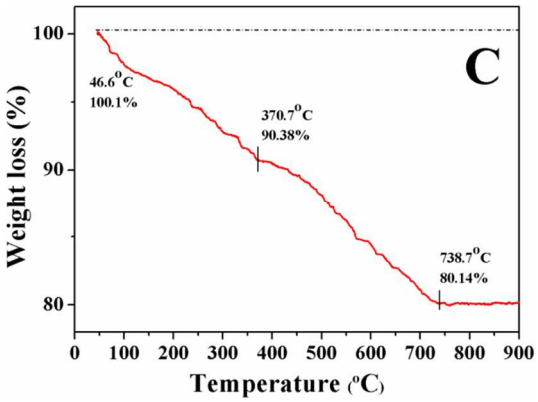

Fig. 5. Thermal decomposition weight loss profiles of Ru(II)-polypyridyl complex grafted silica nanohybrids I (A), II (B) and $Ag@SiO_2$ core-shell nanohybrid III (C) under N_2 gas flow.

Thermogravimetric analyses (TGA) were carried out to determine the presence of covalently grafted Ru(II)-polypyridyl complexes and their stability over wide temperature range (35˚-900˚C) under N_2 gas flow. Thermal decomposition initial onset was noted at 439.6˚C with 93.72% weight loss. The initial weight loss at ≤ 439.6˚C was assigned to dehydration process from silica nanohybrid I. This single stage decomposition started at 439.6˚C and ended at 891.3˚C with 66.79% weight loss and was assigned to the decomposition of 3-APTMS coupled Ru(II)(2,2'-bpy)$_2$(IPBA).2PF$_6$ (net weight loss change 26.9%). Similarly, for silica nanohybrid II, the initial thermal decomposition onset was at 427.7˚C with 90.89% and ended at 899.3˚C with 79.63% weight loss and was assigned to thermal decomposition of 3-APTMS coupled Ru(II)(1,10-phen)$_2$(IPBA).2PF$_6$. Whereas, $Ag@SiO_2$ core-shell nanohybrid III showed multi-stage thermal decomposition, at 370.7˚C with 90.38% weight loss and another at 738.7˚C with 80.14% weight loss. These thermal decomposition weight loss profiles confirmed the presence of covalently grafted Ru(II)-polypyridyl complexes on SiO_2 surface. Moreover, the higher thermal stability of silica nanohybrids I and II is due to the presence of amide surface linking group (-CONH-) than covalently grafted Ru(II)(3,4,7,8-tetramethyl-1,10-phen)$_2$(IPP).2PF$_6$ on $Ag@SiO_2$ core-shell nanohybrid III with ether surface linking group (Ar-O-CH_2) (Fig. 5). Furthermore, Ru(II)-polypyridyl complexes before and after silylating with a 3-APTMS coupling agent in methanolic solution and the resulting silica nanohybrids after grafting over SiO_2 NPs were dispersed in DMSO in order to study optical properties of functionalized silica nanohybrids (Fig. 6). Since, SiO_2 NP surface imitates silicon native oxide layer (p^+ Si-wafer), its high dispersing ability in DMSO enables optical probing studies using UV-vis spectroscopy.[37] The resulting UV-vis spectral data clearly showed the formation of 3-APTMS coupled Ru(II)-polypyridyl complexes with red shift in MLCT from 456 nm to 460 nm and 451 nm to 456 nm (Fig. 6A, 6C). This red shift in MLCT band continued after grafting on SiO2 NP surface (Fig. 6B, 6D). In UV-vis spectra of Ru(II)(3,4,7,8-tetramethyl-1,10-phen)2(IPP).2PF6 complex exhibits an MLCT band at 426 nm (Fig. 6E) and citrate capped Ag NP showed SPR band at 438 nm (Fig. S1). The LSPR coupling from Ag NP led to the enhanced absorption cross-section of Ru(II) (3,4,7,8-tetramethyl-1,10-phen)2(IPBA).2PF6 complex (Fig. 6F).

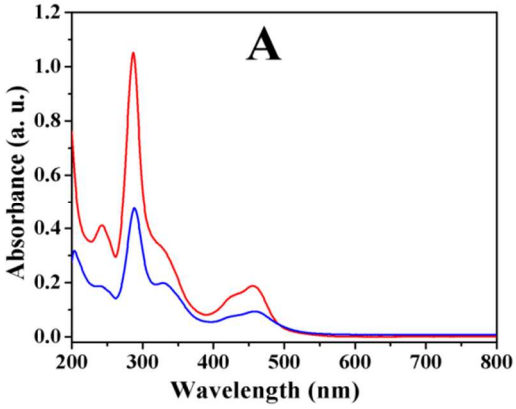

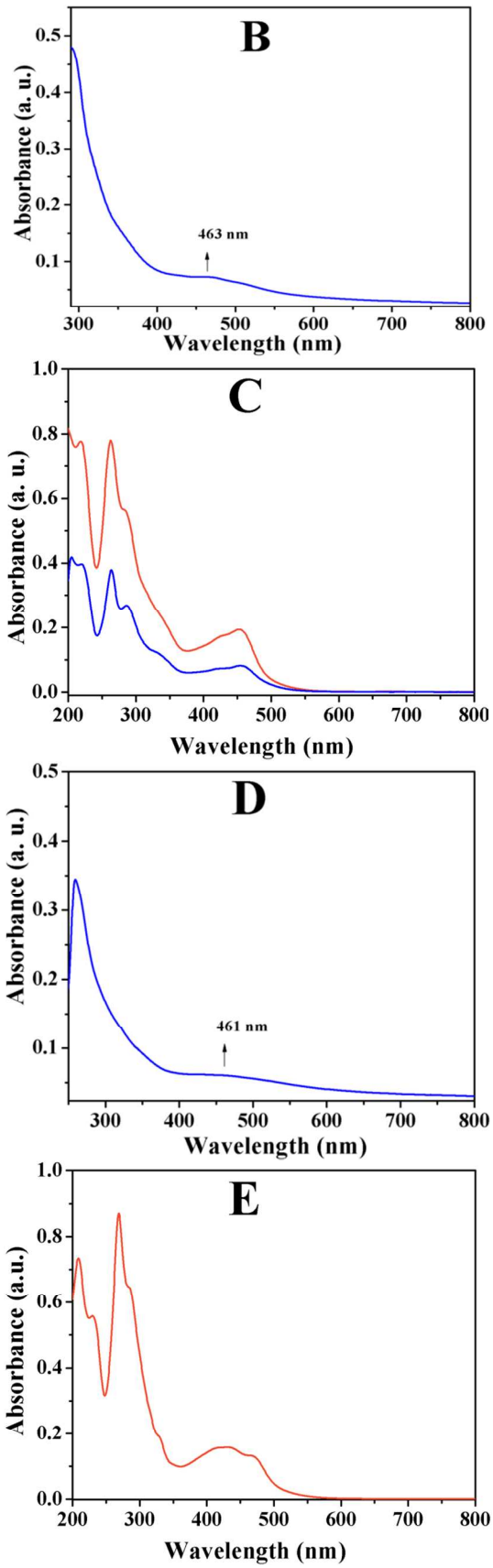

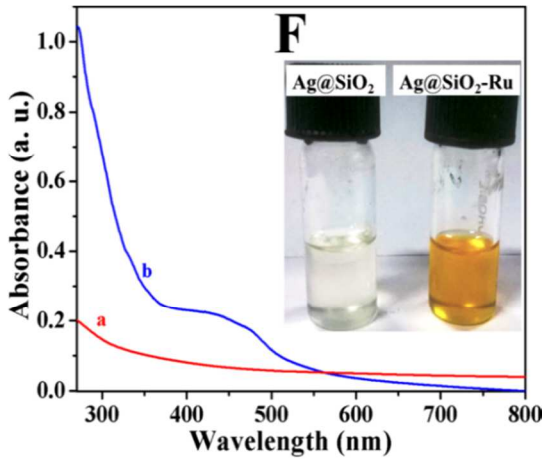

Fig. 6. A) UV-vis spectra of Ru(2,2'-bpy)$_2$(IPBA).2PF$_6$ in solution (red, 10^{-5} M) and after coupling with 3-APTMS (blue); B) Ru(2,2'-bpy)$_2$ (IPBA).2PF$_6$ complex grafted Si-RuH1 nanohybrid I in DMSO with MLCT at 463±1 nm; C) Ru(1,10-phen)$_2$(IPBA).2PF$_6$ in solution (red, 10^{-5} M) and after coupling with 3-APTMS (blue); D) Si-RuH2 nanohybrid II in DMSO showing MLCT at 461 nm; E) Ru(II)(3,4,7,8-tetramethyl-1,10-phen)$_2$(IPP).2PF$_6$ in acetonitrile (red, 10^{-5} M); F) UV-vis spectra of bare Ag@SiO$_2$ core-shell NPs before (a) and after grafting 3-IPTMS coupled Ru(II)(3,4,7,8-tetramethyl-1,10-phen)$_2$(IPP).2PF$_6$ complex in DMSO (b); inset shows digital image of bare Ag@SiO$_2$ core-shell NPs (colourless) and Ag@SiO$_2$ core-shell nanohybrid III in DMSO (yellow).

In addition, mass fragmentation studies evidenced the formation of 3-APTMS coupled Ru(II)(2,2'-bpy)$_2$(IPBA).2PF$_6$ by showing peak at *m/z* 377.3173 (calc.= 368.48) and 3-APTMS coupled Ru(II)(1,10-phen)$_2$(IPBA).2PF$_6$ peak at *m/z* 493.3834 (calc.= 493.05) (Fig. S6-S7). 3-IPTMS linked Ru(II)(3,4,7,8-tetramethyl-1,10-phen)$_2$(IPBA).2PF$_6$ grafted on Ag@SiO$_2$ core-shell nanohybrid III showed peak at *m/z* 885.146 (calc.= 888.277) and shows corresponding fragment patterns of grafted Ru(II)(3,4,7,8-tetramethyl-1,10-phen)$_2$(IPBA).2PF$_6$ (Fig. S8-S9).

These combined studies from various analytical techniques clearly demonstrated the successful stepwise covalent grafting of Ru(II)-polypyridyl complexes on SiO$_2$ surface with and without Ag NP core. Additionally, the influence of Ag NP core over optical performance of Ag@SiO$_2$ nanohybrid III was analysed by emission study in solution and solid state. Ru(II)(3,4,7,8-tetramethyl-1,10-phen)$_2$(IPP).2PF$_6$ complex in acetonitrile (10^{-5} M) showed emission at 620 nm, but after grafting on Ag@SiO$_2$ NP surface, emission shifted to 625 nm (bathochromic shift). Here, Ag NP SPR enhanced the emission of Ru(II)(3,4,7,8-tetramethyl-1,10-phen)$_2$(IPP).2PF$_6$ grafted on Ag@SiO$_2$ core-shell nanohybrid III (Fig. 7), whereas no such enhanced emission is noticed for remaining Ru(II)-polypyridyl complexes in solution and silica nanohybrids I, II (Fig. S10 and Fig. S11). Solid state PL studies of silica nanohybrid I, II and Ag@SiO$_2$ core-shell nanohybrid III were showed luminescence band maxima at 630 nm, 665 nm and 660 nm respectively (Fig. 7B). This significant photo-physical property of Ag@SiO$_2$ core-shell nanohybrid III arises because of the presence of larger Ag NP core with thick SiO$_2$ nanoshell, which limits direct charge transfer from the excited state Ru(II)-centre to Ag NP core in addition to LSPR and scattering effect of Ag NP.[17,38]

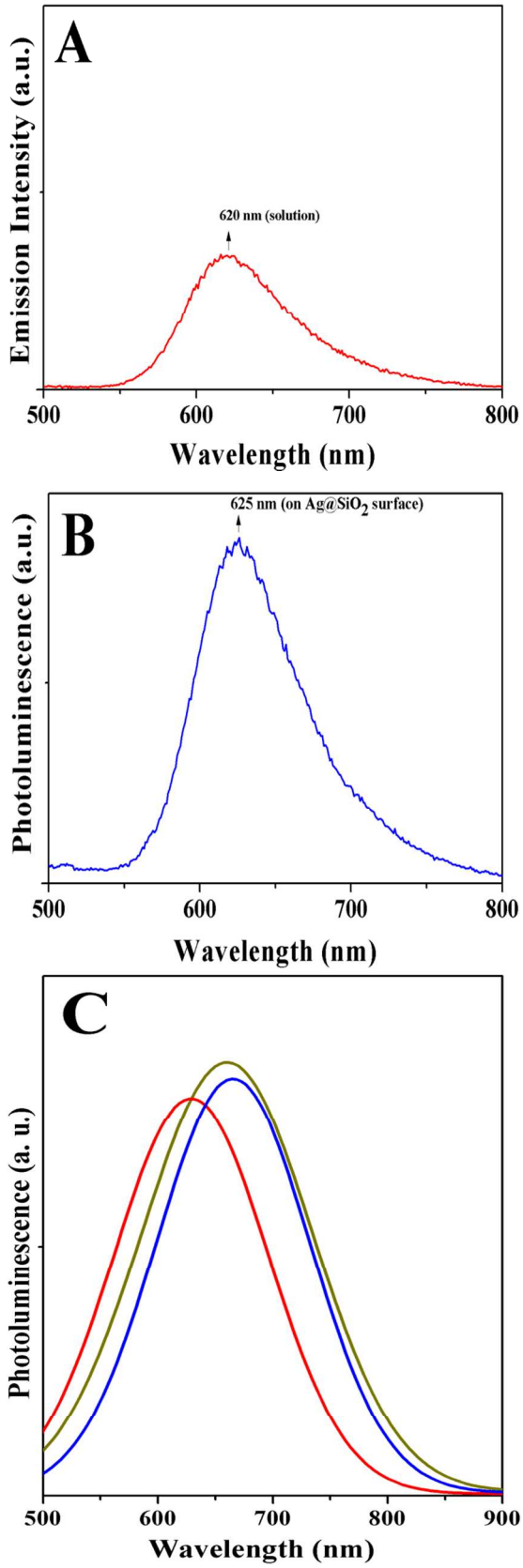

Fig. 7. A) Emission spectra of 10^{-5} M Ru(II)(3,4,7,8-tetramethyl-1,10-phen)$_2$(IPP).2PF$_6$ in acetonitrile (red, λ_{em} = 620 nm); B) Photoluminescence (PL) of Ag@SiO$_2$ core-shell nanohybrid III (blue, λ_{em} = 625 nm) in DMSO (~250 µg in 2 ml); C) Solid state photoluminescence (PL) profiles of silica nanohybrid I (red, λ_{em} = 630 nm), silica nanohybrid II (blue, λ_{em} = 665 nm) and Ag@SiO$_2$ core-shell nanohybrid III (green, λ_{em} = 660 nm).

By taking the advantage of plasmonic Ag NP core in Ag@SiO$_2$ core-shell nanohybrid III, covalently grafted Ru(II)(3,4,7,8-tetramethyl-1,10-phen)$_2$(IPP).2PF$_6$ molecular structural vibrations were studied using Raman spectroscopy with different laser excitation wavelengths (488 nm, 785 nm) at different laser exposure time period at the same focal point.[39] Thanks to larger Ag NP core, which acts as "plasmonic hot spot" to enhance molecular vibrations of covalently grafted Ru(II)(3,4,7,8-tetramethyl-1,10-phen)$_2$(IPP).2PF$_6$ in the controlled fashion with respect to exposure time (Fig. 8c and Fig. S12A).

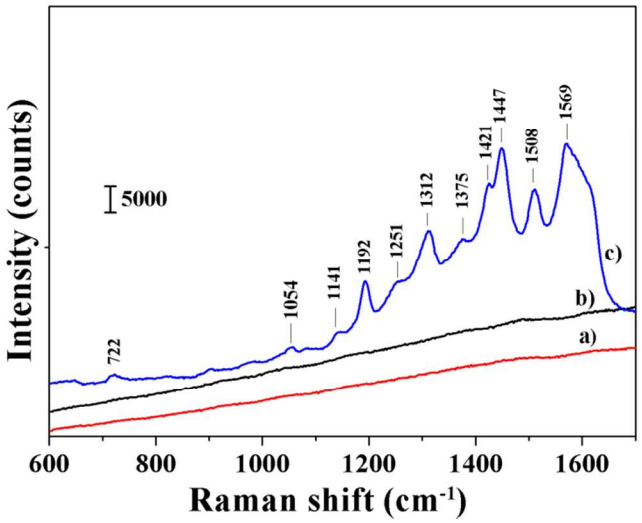

Fig. 8. a) Raman scattering spectrum of silica nanohybrid I; b) silica nanohybrid II; c) Ag NP plasmon enhanced Raman scattering (PERS) spectrum of Ag@SiO$_2$ core-shell nanohybrid III (λ_{ex} = 488 nm).

The band at 722 cm^{-1} noticed from large displacement of N-atom, 902 and 1054 cm^{-1} are assigned to in-plane angular deformation mode of C-H with 3,4,7,8-tetramethyl-1,10-phen ring breathing mode. Ag NP plasmon enhanced Raman scattering (PERS) bands at 1141, 1192, 1251, 1312, 1375, 1421, 1447 cm^{-1} are assigned to IPP ligand. The bands at 1508, 1569 and 1615 cm^{-1} originated from stretching modes of both 3,4,7,8-tetramethyl-1,10-phen and IPP ligands.[40-41] Here, the intensity of vibrational bands (C-C and C-N) of Ru(II)(3,4,7,8-tetramethyl-1,10-phen)$_2$(IPP).2PF$_6$ from 1300-1600 cm^{-1} experienced more electron transfer (Ru-d-orbital to π-system of 3,4,7,8-tetramethyl-1,10-phen) on Ag@SiO$_2$ core-shell nanohybrid III. Exposure time dependent Raman scattering studies clearly demonstrated that, 488 nm laser excitation acts as on-resonance excitation for Ag@SiO$_2$ core-shell nanohybrid III. Because, no such enhanced Raman scattering effect was observed at 785 nm laser excitation with different laser exposure time periods (10 s, 60 s) (Fig. S12B). Similarly, Raman scattering bands are not observed for silica nanohybrids I, II due to the absence of Ag NP core (Fig. 8). This study clearly stresses more on the important role of Ag NP plasmon in the determination of structural information of molecules by grafting near Ag NP surface.

3.1. Photocatalytic activity of silica nanohybrids on Rhodamine 6G degradation

To show the photocatalytic activity of Ru(II)-polypyridyl complex functionalized silica nanohybrids for the decomposition of organic pollutants, we performed experiments by taking Rhodamine 6G as a model organic pollutant. Furthermore, bare MCM-41 SiO_2 NP without functionalization is utilized as a photocatalytic reference to understand the presence and influence of Ag NP core in functionalized $Ag@SiO_2$ core-shell nanohybrid. Plasmonic photocatalytic activity of Ag NP with SiO_2 is well known and has greater impact on the visible light energy conversion in the dye sensitized solar cells processes.[42]

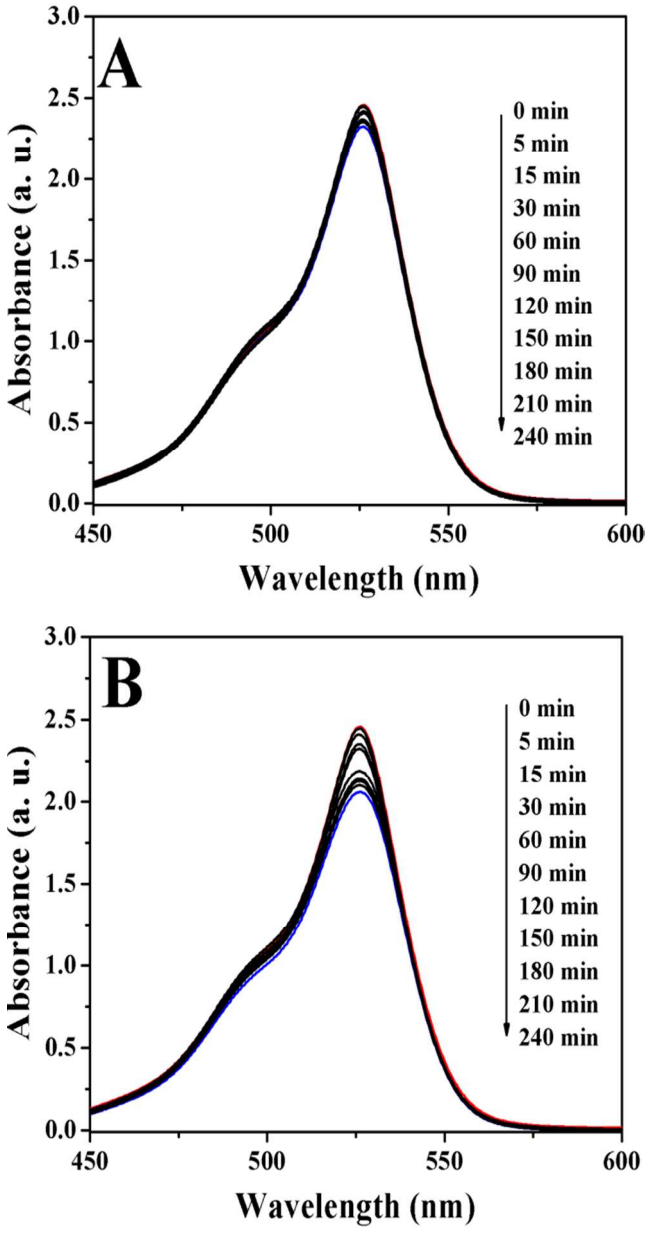

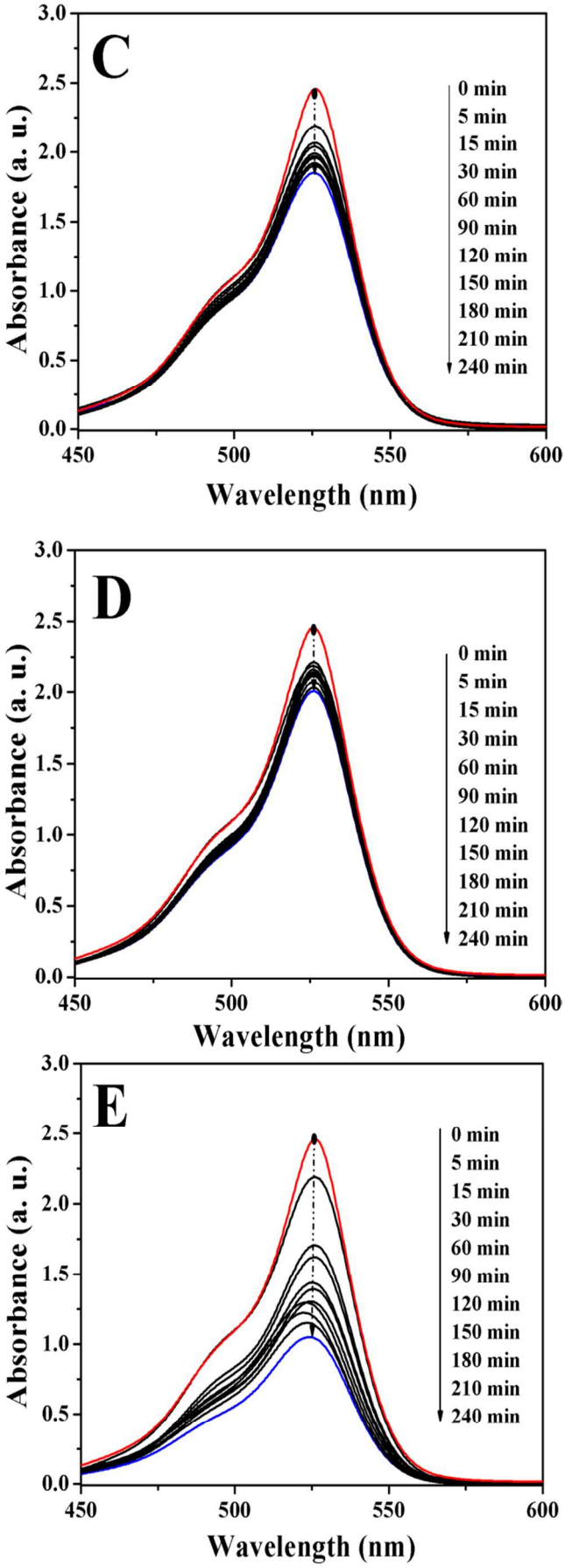

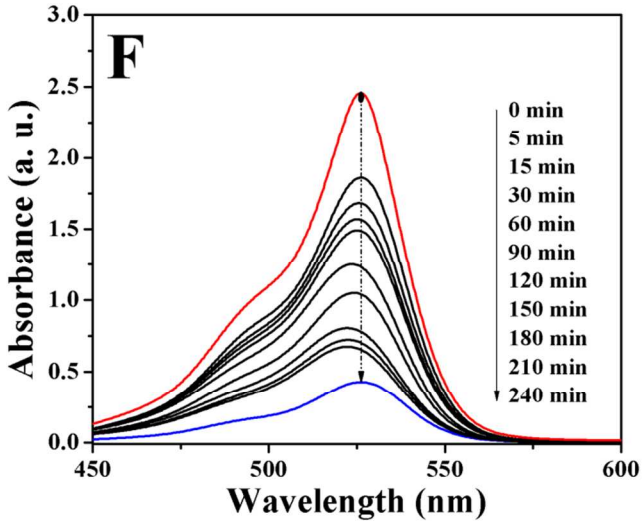

Fig. 9. Photocatalytic activity of silica nanohybrids on Rhodamine 6G decomposition: A) no catalyst; B) MCM-41 SiO_2 NP; C) Si-RuH1 nanohybrid I; D) Si-RuH2 nanohybrid II; E) Blank Ag@SiO_2 core-shell NP; F) Ag@SiO_2 core-shell nanohybrid III.

In order to analyse the degradation ability of Ru(II)-polypyridyl complex functionalized silica nanohybrids I, II and III with Ag NP core, visible light (>400 nm) was chosen as the light source. Control experiment was performed in the absence of photocatalysts to find out the individual role of SiO_2 NP (Fig. 9A). Ag@SiO_2 core-shell nanohybrid III showed enhanced photocatalytic activity than other silica nanohybrids I, II and pure ~120 nm MCM-41 SiO_2 NP (Fig. 9B-F). Also, there is no significant degradation of Rhodamine 6G in the absence of photocatalysts and in the presence of MCM-41 SiO_2 NP. The overall degradation profile of Rhodamine 6G by different functionalized silica nanohybrids (Fig. 10) proved that Ag@SiO_2 nanohybrid III decomposed > 80 % whereas blank Ag@SiO_2 core-shell NPs without Ru(II)-polypyridyl complex decomposed 57% in 240 minutes under visible light illumination. In case of no Ru(II) complexes on Ag@SiO_2, plasmonic surface scattering of large Ag NP core plays key role in photocatalytic process and might provide the driving energy for photocatalytic active species from SiO_2 silanol (-Si-OH) functional group.[8,15] Therefore, the strong plasmon effect and surface scattering effect from bare Ag@SiO_2 NP showed remarkable photocatalytic activity on Rhodamime 6G decomposition. Therefore, the efficient degradation of Rhodamine 6G is possible under visible light in the presence of functionalized Ag@SiO_2 core-shell nanohybrid III. Most importantly, it is noticed that Ag@SiO_2 core-shell nanohybrid III isolated and recovered simply by sedimentation and would greatly supports the practical application to decompose organic wastes from contaminated water. Thus, enhancement in photocatalytic activity of Ag@SiO_2 core-shell nanohybrid III due to Ag NP LSPR as well as energy transfer through non-radiative process with excited Ru(II)-centre was observed. Covalently grafted Ru(II)(3,4,7,8-tetramethyl-1,10-phen)$_2$(IPP).2PF_6 on Ag@SiO_2 core-shell nanohybrid could absorb visible light and causes generation of excited singlet metal-to-ligand charge transfer (^{1}MLCT) state, which further goes through intersystem crossing and generates triplet MLCT state (^{3}MLCT).[43-44] This excited MLCT state favoured the formation of reactive oxygen species like singlet oxygen ($^1O_2$), superoxide anion ($O_2^{\cdot-}$) through electron-transfer to molecular oxygen (O_2). Additionally, the presence of Ag NPs LSPR could enhance the excitation rate of surface bound Ru(II)(3,4,7,8-tetramethyl-1,10-phen)$_2$(IPP).2PF_6 complex. This factor may increase the electron-transfer rate toward O_2 and thus leads to enhancement of the photocatalytic activity.[45]

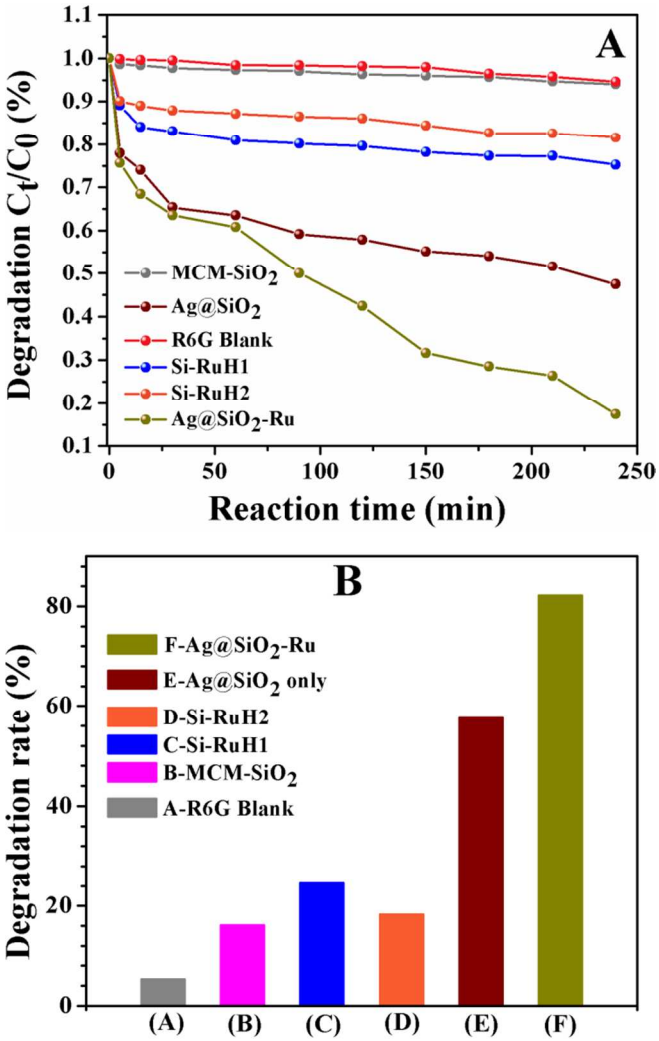

Fig. 10. A) Photocatalytic decomposition profile of Rhodamine 6G; B) Photocatalytic degradation rate of Rhodamine 6G in presence of different Ru(II)-polypyridyl complex grafted silica nanohybrids and control experiment without any photocatalysts.

4. Conclusions

Silica nanohybrids with different Ru(II)-polypyridyl complexes were prepared and their optical studies were performed in solution, on SiO_2 NP surface and Ag@SiO_2 core-shell NP surface. Covalently grafted photoactive Ru(II)-polypyridyl complexes on SiO_2 surface ensured leach-free optoplasmonic properties in solution and solid state. Time dependent enhancement of Raman scattering showed the importance as well as influence of Ag NP LSPR on probing structural vibrations of covalently grafted Ru(II)(3,4,7,8-tetramethyl-1,10-

phen)$_2$(IPP).2PF$_6$ complex. The presence of Ag NP core with SiO$_2$ nanoshell proved as an efficient and heterostructured interface for enhanced photophysical performance along with organic pollutant decomposition.[46] In photocatalysis, the decomposition of Rhodamine 6G was performed in presence of visible light, which provides more advantages than injurious UV-light irradiation. Among functionalized silica nanohybrids I, II and III, Ru(II)(3,4,7,8-tetramethyl-1,10-phen)$_2$(IPP).2PF$_6$ complex grafted Ag@SiO$_2$ nanohybrid III showed Ag NP surface plasmon enhanced optoplasmonic effect in solution and solid state with remarkable photocatalytic activity on Rhodamine 6G decomposition and illustrated the importance of surface engineering of core-shell hybrid materials for the plasmon coupling based energy transfer systems[47] and environment remedial prospects.

Acknowledgements

NV acknowledges DST Nanomission (SR/NM/NS-12/2010), Govt. of India, India for financial support and CSIR-NIPER, Mohali, India for providing HRTEM facility and Mr. Cecil Antony for providing centrifugation facility.

Notes and references

[a] *Chemical Biology Laboratory, Department of Chemistry, University of Delhi, New Delhi-110007, India. Tel: +91-9582087608; E-mail: skawasthi@chemistry.du.ac.in*

[b] *Faculty of Life Sciences and Biotechnology, South Asian University, New Delhi-110021, India. Tel: +91-9999074473; E-mail: rdgupta@sau.ac.in*

†Dedicated to Late Dr. Tarkeshwar Gupta

Electronic supplementary Information (ESI): [Fig. S1. UV-vis spectral profile of citrate capped Ag NPs and TEM image with SAED; Fig. S2 EDS and FFT profile of Ag@SiO$_2$ core-shell NPs without surface functionalization; Fig. S3A,B. FT-IR spectra of Ru(3,4,7,8-tetramethyl-1,10-phen)$_2$(IPP).2PF$_6$ complex and Ag@SiO$_2$ core-shell NPs (a) and (b) after grafting 3-IPTMS linked Ru(3,4,7,8-tetramethyl-1,10-phen)$_2$(IPP).2PF$_6$; Fig. S4. A) FT-IR spectra of Ru(2,2'-bpy)$_2$(IPBA).2PF$_6$ complex (a) before and (b) after silylating with 3-APTMS, B) Ru(1,10-phen)$_2$(IPBA).2PF$_6$ complex (a) before and (b) after silylating with 3-APTMS; Fig. S5. A, B, C) TEM image with SAED, SEM image of MCM-41 SiO$_2$ NPs, amorphous SiO$_2$ without surface functionalization; Fig. S6. Mass spectra of Ru(2,2'-bpy)$_2$(IPBA).2PF$_6$ before and after linked with 3-APTMS; Fig. S7. Mass spectra of Ru(1,10-phen)$_2$(IPBA).2PF$_6$ before and after linked with 3-APTMS; Fig. S8. Mass spectrum of Ru(3,4,7,8-tetramethyl-1,10-phen)$_2$(IPP).2PF$_6$ in acetonitrile; Fig. S9. Mass spectrum of Ru(3,4,7,8-tetramethyl-1,10-phen)$_2$(IPP).2PF$_6$ grafted Ag@SiO$_2$ nanohybrid III; Fig. S10. Emission spectra of 10^{-5} M Ru(2,2'-bpy)$_2$(IPBA).2PF$_6$ and Ru(1,10-phen)$_2$(IPBA).2PF$_6$ in acetonitrile; Fig. S11. Emission spectra of Ru(2,2'-bpy)$_2$(IPBA).2PF$_6$ and Ru(1,10-phen)$_2$(IPBA).2PF$_6$ complex functionalized silica nanohybrid I and II in DMSO; Fig. S12. Raman scattering spectra of Ag@SiO$_2$ core-shell nanohybrid III A) λ_{exc} = 488.0 nm (on-resonance proof); B) λ_{exc} = 785.0 nm (off-resonance proof)].

1 a) M. K. Gangishetty, K. E. Lee, R. W. J. Scott and T. L. Kelly *ACS Appl. Mater. Interfaces* 2013, **5**, 11044-11051; b) W. Zhao, N. Du, C. Xiao, H. Wu, H. Zhang and D. Yang *J. Mater. Chem. A*, 2014, **2**, 13949-13954.

2 A. Burns, H. Ow and U. Wiesner *Chem. Soc. Rev.,* 2006, **35**, 1028-1042.

3 a) G. Satishkumar, M. V. Landaub, T. Buzaglob, L. Frimetb, M. Ferentzb, R. Vidrukb, F. Wagnerc, Y. Galb and M. Herskowitz *Appl. Catal., B* 2013, **138**, 276-284; b) Y. Li, L. Yao, Y. Song, S. Liu, J. Zhao, W. Ji and C-T. Au *Chem. Commun.,* 2010, **46**, 5298-5300.

4 H. Goesmann and C. Feldmann *Angew. Chem. Int. Ed.,* 2010, **49**, 1362-1395.

5 A. Fashina, E. Antunes and T. Nyokong *New J. Chem.,* 2013, **37**, 2800-2809.

6 G. Alberto, G. Caputo, G. Viscardi, S. Coluccia and G. Martra *Chem. Mater.* 2012, **24**, 2792-2801.

7 O. Niitsoo and A. Couzis *J. Colloid Interface Sci.,* 2011, **354**, 887-890.

8 L. Q. Xu, B. S. M. Yap, R. Wang, K-G. Neoh, E-T. Kang and G. D. Fu *Ind. Eng. Chem. Res.*, 2014, **53**, 3116-3124.

9 a) X. Yang, H. Zhong, Y. Zhu, H. Jiang, J. Shen, J. Huang and C. Li *J. Mater. Chem. A,* 2014, **2**, 9040-9047; b) R. Poreddy, E. J. García-Suárez, A. Riisager and S. Kegnaes *Dalton Trans.*, 2014, **43**, 4255-4259.

10 M. Wu, B. F. Yang, Y. Lv, Z. P. Fu, J. A. Xu, T. Guo and Y. X. Zhao *Appl. Surf. Sci.* 2010, **256**, 7125-7130.

11 Y. Yan, H. Sun, P. Yao, S-Z. Kang, J. Mu *Appl. Surf. Sci.* 2011, **257**, 3620-3626.

12 Y-C. Liang, C-C. Wang, C-C. Kei, Y-C. Hsueh, W-H. Cho and T-P. Perng *J. Phys. Chem. C,* 2011, **115**, 9498-9502.

13 K. Xie, L. Suna, C. Wanga, Y. Lai, M. Wanga, H. Chena and C. Lin *Electrochimica Acta* 2010, **55**, 7211-7218.

14 P. Wang, M. Du, M. Zhang, H. Zhua and S. Bao *Dalton Trans.*, 2014, **43**, 4255–4259.

15 K. Awazu, M. Fujimaki, C. Rockstuhl, J. Tominaga, H. Murakami, Y. Ohki, N. Yoshida and T. Watanabe *J. Am. Chem. Soc.* 2008, **130**, 1676-1680.

16 F. Liu, B. S. Rao and J-M. Nunzi *Organic Electronics* 2011, **12**, 1279–1284.

17 H. Mishra, B. L. Mali, J. Karolin, A. I. Dragan and C. D. Geddes *Phys. Chem. Chem. Phys.*, 2013, **15**, 19538-19544.

18 N. Vilvamani, T. Gupta, R. D. Gupta and S. K. Awasthi *RSC Adv.,* 2014, **4**, 20024.

19 V. Singh, P. C. Mondal, A. Kumar, Y. L. Jeyachandran, S. K. Awasthi, R. D. Gupta and M. Zharnikov *Chem. Commun.,* 2014, DOI: 10.1039/C4CC05063K.

20 F. Lupo, M. E. Fragala, T. Gupta, A. Mamo, A. Aurelianao, M. Bettinelli, A. Speghini and A. Gulino *J. Phys. Chem. C* 2010, **114**, 13459-13464.

21 T. Gupta, E. Tartakovsky, M. A. Iron and M. E. van der Boom *ACS Appl. Mater. Interfaces* 2010, **2**, 7-10.

22 M-J. Li, Z. Chen,V. W-W. Yam and Y. Zu *ACS Nano,* 2008, **2**, 905-912.

23 D. B. G. Williams and M. Lawton *J. Org. Chem.* 2010, **75**, 8351-8354.

24 W. Paw and R. Eisenberg *Inorg. Chem.* 1997, **36**, 2287-2293.

25 Y-C. Hsu, H. Zheng, J. T. Lin and K-C. Ho *Sol. Energy Mater. Sol. Cells* 2005, **87**, 357-367.

26 W. J. Mei, J. Liu, K. C. Zheng, L. J. Lin, H. Chao, A. X. Li, F. C. Yun and L. N. Ji *Dalton Trans.,* 2003, 1352-1359.

27 B. P. Sullivan, D. J. Salmon and T. J. Meyer *Inorg. Chem.* 1978, **17**, 3334.

28 J-F. Yin, D. Bhattacharya, P. Thanasekaran, C-P. Hsu, T-W. Tseng and K-L. Lu *Inorg. Chim. Acta* 2009, **362**, 5064-5072.

29 Q. Cai, Z-S. Luo, W-Q. Pang, Y-W. Fan, X-H. Chen and F-Z. Cui *Chem. Mater.* 2001, **13**, 258-263.

30 S. Cousinie, L. Mauline, M. Gressier, S. R. Kandibanda, L. Datas, C. Reber and M-J. Menu *New J. Chem.,* 2012, **36**, 1355-1367.

31 N. Wangoo, G. Shekhawat, J-S. Wu, A. K. K. Bhasin, C. R. Suri, K. K. Bhasin and V. Dravid *J. Nanopart. Res.* 2012, **14**,1011.

32 Y. Kim, H-B. Kim and D-J. Jang *J. Mater. Chem. A*, 2014, DOI:10.1039/c3ta15177h; b) M. Horecha, E. Kaul, A. Horechyy and M. Stamm *J. Mater. Chem. A*, 2014, DOI:10.1039/C4TA00606B.

33 K. C. Grabar, R. G. Freeman, M. B. Hommer and M. J. Natan *Anal. Chem.* 1995, **67**, 735-743.

34 S. Wang, B. Li, L. Zhang, L. Liu and Y. Wang *Appl. Organometal. Chem.* 2011, **25**, 21-26.

35 Y. Deligiannakis, G. A. Sotiriou and S. E. Pratsinis *ACS Appl. Mater. Interfaces* 2012, **4**, 6609-6617.

36 T. Engel and G. Kickelbick *Chem. Mater.*, 2013, **25**, 149-157.

37 S. Kabehie, M. Xue, A. Z. Stieg, M. Liong, K. L. Wang and J. I. Zink *J. Am. Chem. Soc.,* 2010, **132**, 15987-15996.

38 a) J. Zhou, F. Ren, S. Zhang, W. Wu, X. Xiao, Y. Liu and C. Jiang *J. Mater. Chem. A,* 2013, **1**, 13128-13138; b) C. Louis, S. Roux, G. Ledoux, C. Dujardin, O. Tillement, B. L. Cheng and P. Perriat *Chem. Phys. Lett.* 2006, **429**, 157-160; c) O. G. Tovmachenko, C. Graf, D. J. van den Heuvel, A. van Blaaderen and H. C. Gerritsen *Adv. Mater.* 2006, **18**, 91-95.

39 a) Y. Zhou and P. Zhang *Phys. Chem. Chem. Phys.,* 2014, **16**, 8791-8794; b) L. Yang, H. Wang, B. Yan and B. M. Reinhard *J. Phys. Chem. C*, 2010, **114**, 4901-4908.

40 a) G. D. Danzer, J. A. Golus and J. R. Kincaid *J. Am. Chem. Soc.* 1993, **115**, 8643-8648; b) Y. M. Jung, J. W. Lim, E. R. Kim, H. Lee and M. S. Lee *Bull. Korean Chem. Soc.* 2001, **22**, 318-320; c) Q. Zeng, R. Marthi, A. McNally, C. Dickinson, T. E. Keyes and R. J. Forster *Langmuir,* 2010, **26**, 1325-1333.

41 a) Y. Halpin, H. Logtenberg, L. Cleary, S. Schenk, M. Schulz, A. Draksharapu, W. R. Browne and J. G. Vos *Eur. J. Inorg. Chem.* 2013, 4291-4299; b) B. Abraham, C. V. Sastri, B. G. Maiya and S. Umapathy *J. Raman Spectrosc.* 2004, **35**, 13-18.

42 H. Choi, J-P. Lee, S-J. Ko, J-W. Jung, H. Park, S. Yoo, O. Park, J-R. Jeong, S. Park and J. Y. Kim *Nano Lett.* 2013, **13**, 2204-2208.

43 K. Mori, M. Kawashima, M. Che and H. Yamashita *Angew. Chem. Int. Ed.,* 2010, **49**, 8598-8601.

44 a) G. D. Hager, and G. A. Crosby *J. Am. Chem. Soc.* 1975, **97**, 7031; b) A. Juris, V. Balzani, F. Barigelletti, S. Campagna, P. Belser and A. V. Zelewsky *Coord. Chem. Rev.,* 1988, **84**, 85.

45 K. Mori, M. Kawashima, K. Kagohara and H. Yamashita *J. Phys.Chem. C*, 2008, **112**, 19449.

46 C. C. Kuo and C. H. Chen *Nanoscale* 2014, **6**, 12805-12813.

47 N. Zohar and G. Haran *Langmuir,* 2014, **30**, 7919-7927.